



HAL
open science

Design and synthesis of thiourea-based derivatives as *Mycobacterium tuberculosis* growth and enoyl acyl carrier protein reductase (InhA) inhibitors

Şengül Dilem Doğan, Miyase Gözde Gündüz, Hilal Doğan, Vagolu Siva Krishna, Christian Lherbet, Dharmarajan Sriram

► To cite this version:

Şengül Dilem Doğan, Miyase Gözde Gündüz, Hilal Doğan, Vagolu Siva Krishna, Christian Lherbet, et al.. Design and synthesis of thiourea-based derivatives as *Mycobacterium tuberculosis* growth and enoyl acyl carrier protein reductase (InhA) inhibitors. *European Journal of Medicinal Chemistry*, 2020, 199, pp.112402. 10.1016/j.ejmech.2020.112402 . hal-02863650

HAL Id: hal-02863650

<https://hal.science/hal-02863650>

Submitted on 3 Dec 2020

HAL is a multi-disciplinary open access archive for the deposit and dissemination of scientific research documents, whether they are published or not. The documents may come from teaching and research institutions in France or abroad, or from public or private research centers.

L'archive ouverte pluridisciplinaire **HAL**, est destinée au dépôt et à la diffusion de documents scientifiques de niveau recherche, publiés ou non, émanant des établissements d'enseignement et de recherche français ou étrangers, des laboratoires publics ou privés.

Design and synthesis of thiourea-based derivatives as *Mycobacterium tuberculosis* growth and enoyl acyl carrier protein reductase (InhA) inhibitors

Şengül Dilem Doğan^{a*}, Miyase Gözde Gündüz^b, Hilal Doğan^a, Vagolu Siva Krishna^c, Christian Lherbet^d, Dharmarajan Sriram^c

^a Department of Basic Sciences, Faculty of Pharmacy, Erciyes University, 38039, Kayseri, Turkey

^b Department of Pharmaceutical Chemistry, Faculty of Pharmacy, Hacettepe University, Sıhhiye, 06100, Ankara, Turkey

^c Department of Pharmacy, Birla Institute of Technology and Science-Pilani, 500078, Hyderabad, India

^d LSPCMIB, UMR-CNRS 5068, Université Paul Sabatier-Toulouse III, 118, route de Narbonne, 236 Cours Eugene Cosserat, 31062, Toulouse Cedex, France

*Corresponding author

Dr. Şengül Dilem Doğan

Address: Erciyes University
Faculty of Pharmacy
Department of Basic Sciences
38039
Kayseri, TURKEY

E-mail address: dogandilem@gmail.com

Phone number: +90 352 2076666-28032

Abstract

Tuberculosis remains the most deadly infectious disease worldwide due to the emergence of drug-resistant strains of *Mycobacterium tuberculosis*. Hence, there is a great need for more efficient treatment regimens. Herein, we carried out rational molecular modifications on the chemical structure of the urea-based co-crystallized ligand of enoyl acyl carrier protein reductase (InhA) (PDB code:5OIL). Although this compound fulfills all structural requirements to interact with InhA, it does not inhibit the enzyme effectively. With the aim of improving the inhibition value, we synthesized thiourea-based derivatives by one-pot reaction of the amines with corresponding isothiocyanates. After the structural characterization using ^1H NMR, ^{13}C NMR, FTIR and HRMS, the obtained compounds were initially tested for their abilities to inhibit *Mycobacterium tuberculosis* growth. The results revealed that some compounds exhibited promising antitubercular activity, MIC values at 0.78 and 1.56 $\mu\text{g/mL}$, combined with low cytotoxicity. Moreover, the most active compounds were tested against latent as well as dormant forms of the bacteria utilizing nutrient starvation model and *Mycobacterium tuberculosis* infected macrophage assay. Enzyme inhibition assay against enoyl-acyl carrier protein reductase identified InhA as the important target of some compounds. Molecular docking studies were performed to correlate InhA inhibition data with *in silico* results. Finally, theoretical calculations were established to predict the physicochemical properties of the most active compounds.

Keywords: Antitubercular; antimycobacterial; enoyl-ACP reductase; molecular modeling; docking

1. Introduction

Tuberculosis (TB) is an infectious pulmonary disease caused by *Mycobacterium tuberculosis* (*M. tuberculosis*) and still remains a major global health-threatening problem although existed for centuries [1]. According to the World Health Organization (WHO), ten million people developed TB in 2018 revealing this disease as the foremost reason of life lost by the cause of a single infectious agent [2]. Despite the approval of new anti-TB drugs such as bedaquiline and delamanid (Figure 1) in addition to the existing traditional ones [3,4], TB treatment continues to be a formidable challenge worldwide.

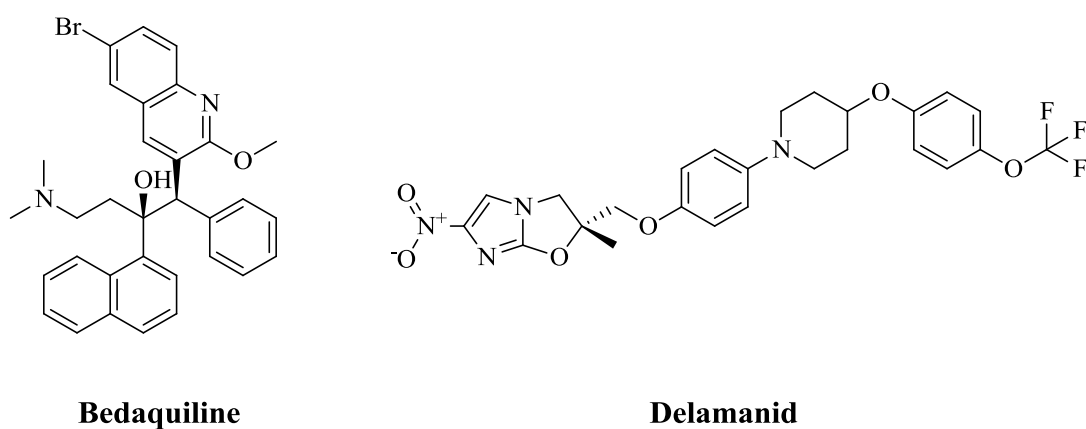


Figure 1. Chemical structures of bedaquiline and delamanid.

The main obstacle to the success of the current TB chemotherapy regime is the emerging extensively drug-resistant and multidrug-resistant tuberculosis as well as the toxicity of the drugs resulting in adverse side effects [5]. Hence, to overcome these problems, the development of new therapeutics with safer toxicity profiles is mandatory.

Thiourea is the classic bioisostere of urea functionality, in which oxygen is replaced by sulfur atom and represents one of the most important core structures incorporated into medicinal chemistry [6,7]. This scaffold serves as an excellent building block in the discovery of new drug candidates with diverse therapeutic applications. There are many commercial examples (Figure 2) that carry thiourea group integrated into their structures such as thiocarlide, thioacetazone (antitubercular), noxytiolin (antibacterial), and thiopental (general anesthetic) [8].

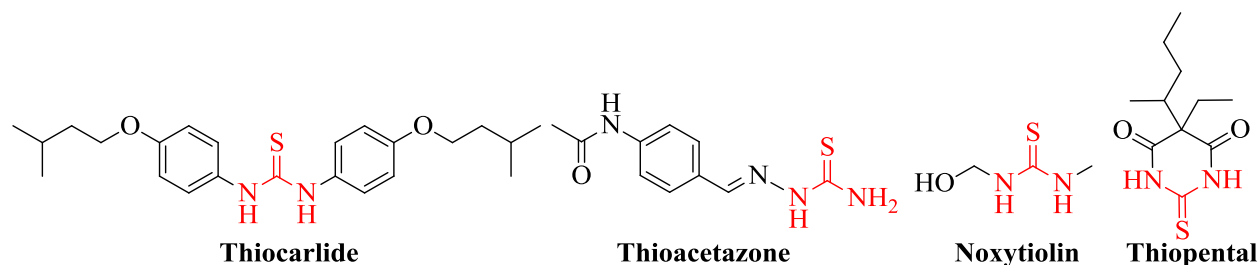


Figure 2. Examples for the drugs carrying thiourea moiety.

Among the above-mentioned commercial ones, thiocarlide (or isoxyl) and thioacetazone are thiourea containing compounds known as effective antitubercular agents against multidrug-resistant strains of *M. tuberculosis*. They interfere with the synthesis of oleic acid, consequently tuberculostearic acid in *M. tuberculosis* affecting mycolic acid synthesis, as well [9]. Both drugs were recently identified to show their mechanism of action by covalently inhibiting HadA component of *M. tuberculosis* fatty acid synthase type II (FAS-II) dehydratase through sulfur atom of thioketone functionality [10].

The enoyl-acyl carrier protein (ACP) reductase, InhA, is an important enzyme employed in the mycolic acid biosynthesis pathway of *M. tuberculosis*. Mycolic acids are long-chain fatty acids and are major components of mycobacterial cell envelope [11]. Therefore, InhA is essential for the growth of *M. tuberculosis* and stands as an attractive target for the discovery of novel antitubercular agents [12].

Although various structurally diverse inhibitors of InhA have been reported (Figure 3), in almost every case, the inhibitors bind to InhA forming interactions with cofactor (NADH), tyrosine amino acid and lipophilic binding pockets of the enzyme [13].

The binding pocket of InhA includes three key regions occupied by the inhibitors. The catalytic site, Site I, contains a tyrosine amino acid and the ribose group of the nicotinamide adenine dinucleotide (NAD) cofactor. The inhibitors interact with the enzyme through hydrogen bonds with the hydroxyl group of Tyr and the ribose ring of NAD. Depending on the chemical structure of the inhibitor, additional hydrogen bond is possible with methionine amino acid. Site II is formed by the hydrophobic pocket near the side chain of Tyr. This site enables the hydrophobic moieties of its inhibitors to bind to InhA via hydrophobic interactions. Site III is comparatively unexplored but the hydrophobic rings of the inhibitors remain close to the phosphate groups of NAD as well as Gly96 and Phe97 at van der Waals distance [14]. These reported interactions of

various ligands with InhA enzyme provide possibilities for the rational design of new inhibitors that can bind to this region.

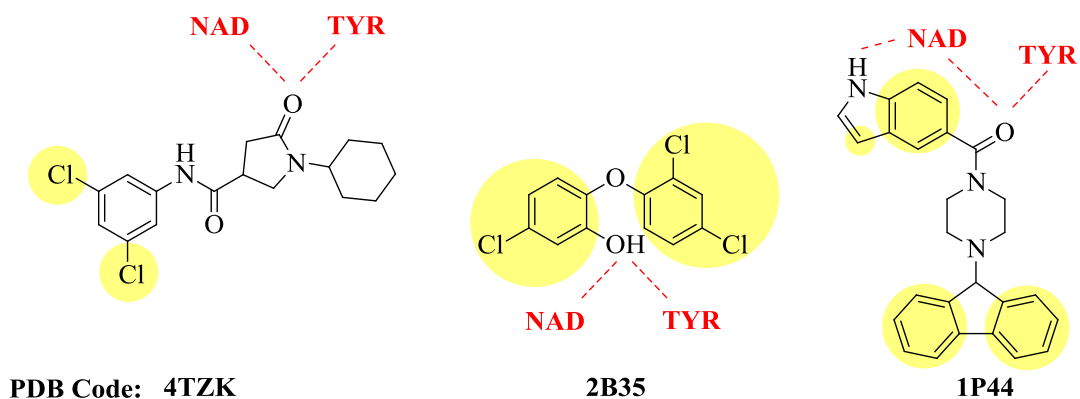


Figure 3. Chemical structures of inhibitors co-crystallized in InhA enzyme. Parts of the molecules participating in InhA binding are highlighted: Hydrogen bonds and hydrophobic interactions are represented as red dotted lines and yellow spheres, respectively.

In 2018, Prati et al. reported several crystal structures of novel InhA–NADH–ligand complexes [15]. One of them contains a urea-based co-crystallized ligand, which is deposited in Protein Data Bank under PDB code 5OIL (Figure 4). Although this compound fulfills all structural requirements to interact with InhA, it is a weak inhibitor at the same time. This situation encouraged us to carry out different modifications on this compound to achieve novel inhibitors capable of targeting InhA.

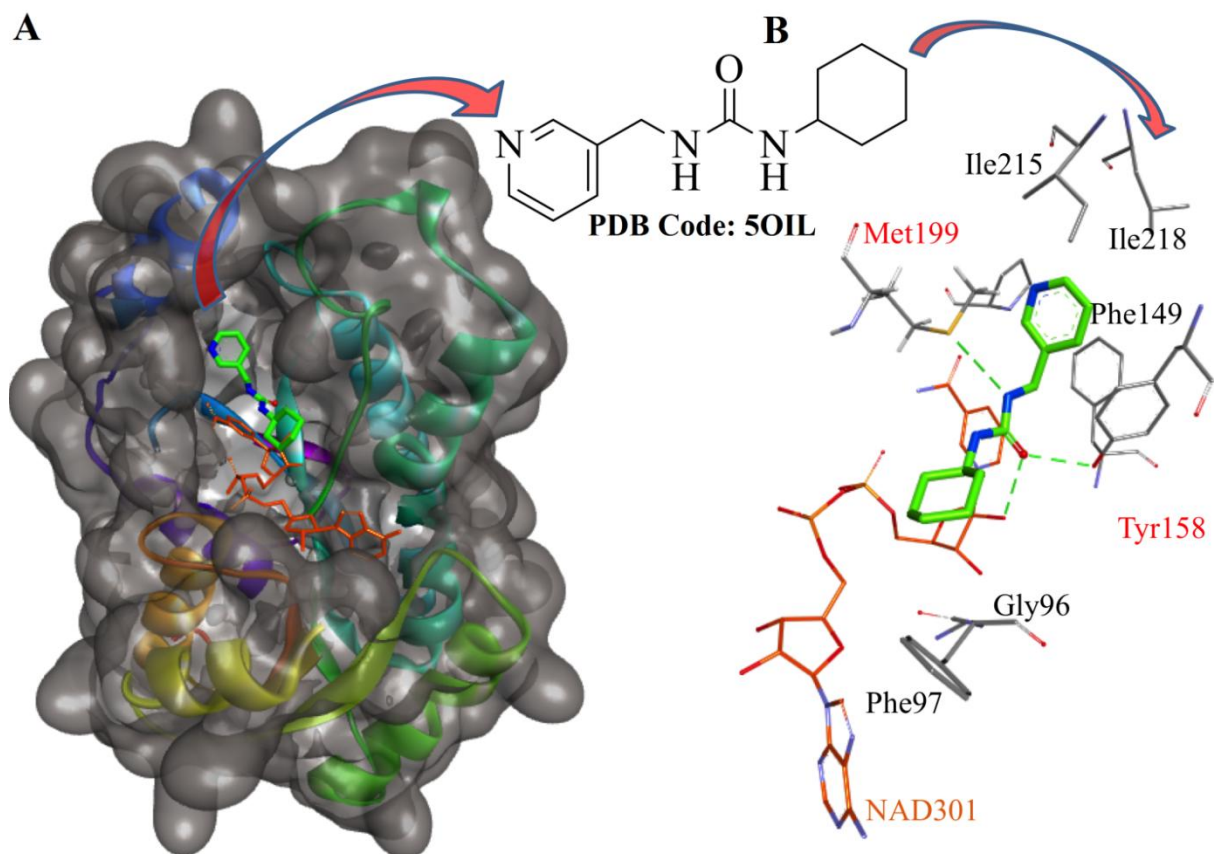


Figure 4. Molecular surface representation of InhA with the co-crystallized ligand and NAD (PDB code:5OIL) shown as green and orange sticks, respectively (A). Expanded view of InhA active pocket: the ligand is represented as green stick, residues providing ligand binding are displayed as lines, hydrogen bonds are shown as green dotted lines (B).

As both urea and thiourea groups possess near-equal molecular volumes and shapes, swapping urea with thiourea is considered to be a rational approach in the drug design process [16,17].

In light of these considerations, we designed and synthesized thiourea derivatives (Figure 5) carrying necessary structural moieties to be *M. tuberculosis* growth and InhA inhibitors. We checked the validity of our hypotheses by various assays on *M. tuberculosis* as well as enzyme inhibition and molecular modeling studies.

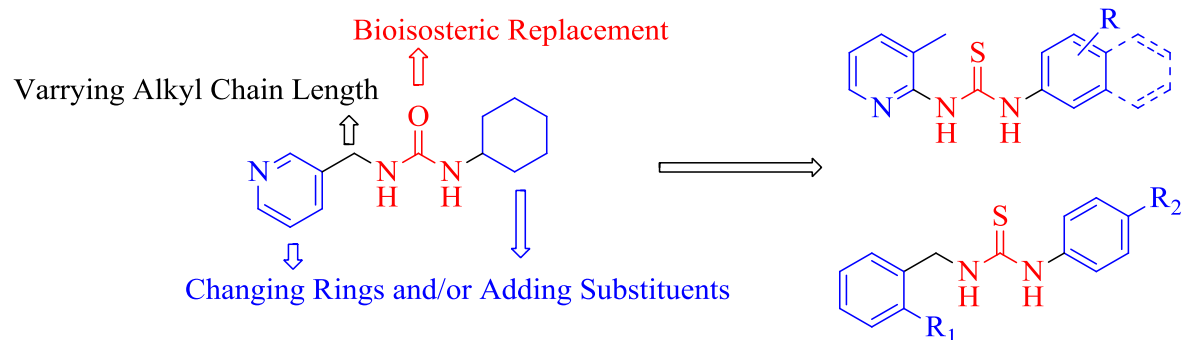


Figure 5. Design strategy for the synthesized compounds

2. Results and discussion

2.1. Synthesis

In the present study, we synthesized two subseries of compounds. Initially, we synthesized *N*-pyridine-*N'*-aryl thiourea derivatives introducing (substituted) phenyl/naphthyl rings into the structure of the compounds (**TU1-TU10**). Subsequently, we obtained benzyl and phenyl substituted thiourea derivatives as the second subseries (**TU11-TU14**). As our aim was to carry out different modifications on the weak inhibitor urea-based ligand of 5OIL to reach more active ones, we swapped the urea functionality with thiourea group in these compounds. To check the validity of this modification, we also added two representative urea derivatives in this subseries (**U1-U2**). The fundamental synthetic path was applied for the synthesis of target compounds **TU1-T14** and **U1-U2**, shown in Figure 6. All compounds were successfully synthesized in a simple one-step method over the reaction of amine with equivalent amount of various isothiocyanate/isocyanate derivatives in toluene at 80 °C. The structures of the target compounds were elucidated by ^1H NMR, ^{13}C NMR, HRMS and FTIR. ^1H NMR and ^{13}C NMR spectra of the synthesized compounds are provided as supplementary materials.

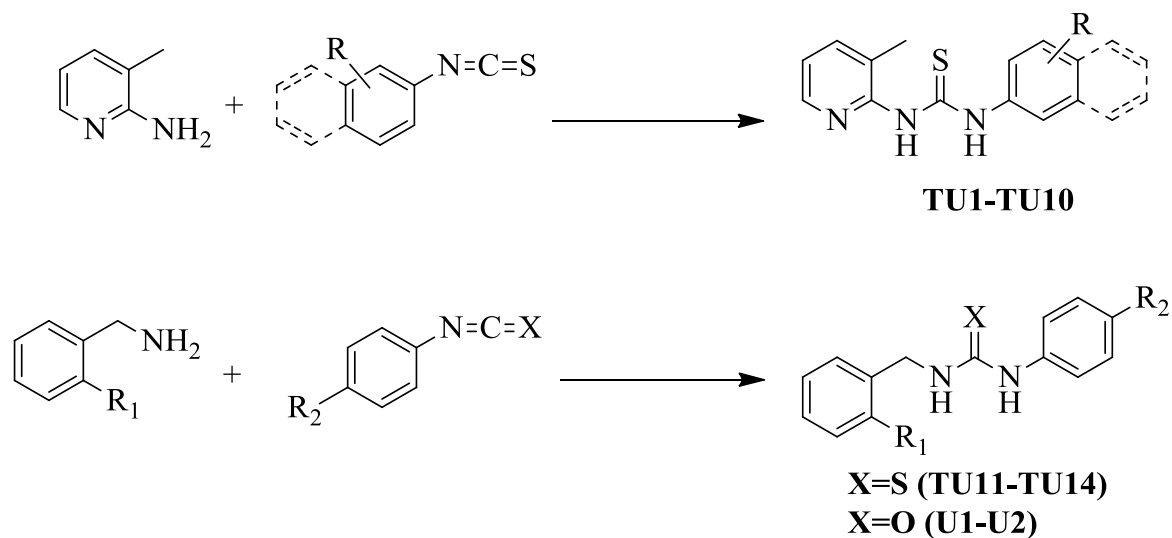


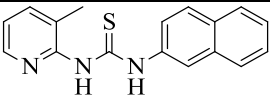
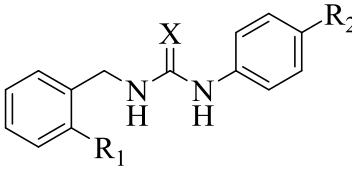
Figure 6. Synthetic pathway for the preparation of target compounds

2.2. *Mycobacterium tuberculosis* growth inhibition and cytotoxicity determination

The minimum inhibitory concentration (MIC) of the synthesized compounds against *M. tuberculosis* H37Rv was determined using Microplate Alamar Blue Assay (MABA) method. Isoniazid, rifampicin, and ethambutol were employed as standard drugs. As cytotoxicity to the healthy cells can emerge a serious problem during the discovery of new antitubercular agents, the most active compounds, possessing MIC values ≤ 1.56 $\mu\text{g/mL}$, were evaluated for the cytotoxic effects using MTT assay. The structures as well as MIC values ($\mu\text{g/mL}$ and μM) of the compounds and the cytotoxicity of the most active derivatives are presented in Table 2.

Table 2. Chemical structures, antitubercular activity and cytotoxicity data of the compounds

Compound	R	MIC ($\mu\text{g/mL}$)	MIC (μM)	Cytotoxicity (% inhibition at 50 $\mu\text{g/mL}$)
TU1	H	>25	>102.88	
TU2	4-OCH ₃	12.5 \pm 1.4	45.79	
TU3	2,4-diCl	0.78\pm0.45	2.50	34.05
TU4	4-Br	0.78\pm0.55	2.42	30.8
TU5	2-CF ₃	>25	>80.39	
TU6	4-CH ₃	25 \pm 0	97.28	
TU7	4-F	12.5 \pm 1.4	47.89	

TU8		4-I		0.78±0.27	2.11	31.19
TU9		3,5-diCF ₃		>25	>65.96	
TU10				>25	>85.32	
						
Compound	X	R₁	R₂	MIC (µg/mL)	MIC (µM)	Cytotoxicity (% inhibition at 50 µg/mL)
TU11	S	Cl	H	>25	>90.25	
TU12	S	Cl	NO ₂	0.78±0.59	2.42	29.86
TU13	S	Br	H	>25	>77.88	
TU14	S	Br	NO ₂	1.56±0.82	4.26	24.93
U1	O	Cl	H	>25	>95.79	
U2	O	Br	H	>25	>81.97	
Isoniazid				0.05±0.02	0.36	
Rifampicin				0.1±0.07	0.12	
Ethambutol				1.56±0.9	7.6	

According to the obtained results, five compounds displayed MIC values at ≤ 1.56 µg/mL and appeared as exceptional antimycobacterial agents. **TU3**, **TU4**, **TU8** and **TU12** stand out with MIC value of 0.78 µg/mL among other derivatives. It is important to emphasize that these compounds are more active than ethambutol, which is among the first-line drugs for tuberculosis treatment. Furthermore, **TU14** showed MIC value at 1.56 µg/mL likewise ethambutol. In the first subseries (**TU1-TU10**) changing the substituents of the phenyl ring played an important role in the mentioned activity. Introducing the chlorine, bromine and iodine atoms led to a great decrease in the MIC values. However, keeping the phenyl/naphthyl ring unsubstituted destroyed the antitubercular effect of the compounds. In the second subseries, it is obvious that nitro group on the phenyl ring made a great contribution to mentioned activity. On the other hand, changing the substituent on the benzyl functionality as bromine or chlorine did not play a role in either urea or thiourea derivatives. Consequently, thiourea derivatives with nitro groups appeared as the most active ones in this subseries. With these results, we also observed that swapping the urea group with thiourea functionality was a logical modification to obtain more active antitubercular agents. As toxicity, particularly hepatic and ocular toxicity, is one of the most important limiting factors of TB treatment with first-line drugs such as isoniazid, rifampicin and ethambutol, it is of utmost

significance to discover new agents with low cytotoxicity [18,19]. In this study, five compounds (**TU3**, **TU4**, **TU8**, **TU12** and **TU14**), which have MIC values $\leq 1.56 \mu\text{g/mL}$, were found to be non-toxic with $<50\%$ inhibition in accordance with cytotoxicity data obtained from MTT assay.

2.3. Nutrient starvation model of *Mycobacterium tuberculosis H37Rv*

While determining the antitubercular activities of the new drug candidates, it is critical to perform the biological experiments on inactive or persistent form of *M. tuberculosis*, which can endure oxygen and supplement deprived conditions. With this aim, a nutrient starvation model was applied on the bacteria by starving the culture in phosphate buffer saline (PBS) for six weeks. Afterward, **TU3**, **TU8** and **TU12**, the representative compounds with the lowest MIC values obtained from MABA, were treated with the culture. The obtained results are provided in Figure 7.

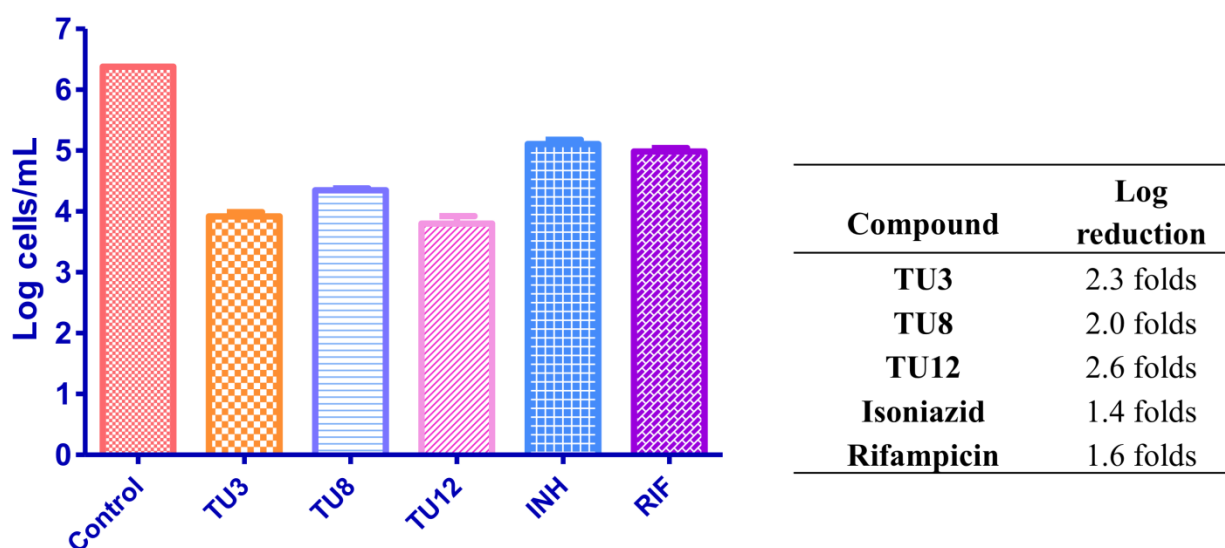


Figure 7. Activity profile of the selected compounds against *M. tuberculosis* in the nutrient starvation model. Bacterial count estimation (Mean \pm S.D., $n = 3$) was conducted using the MPN (most probable number) assay. Significance plot was generated using two way ANOVA ($p < 0.0001$, GraphPad Prism Software).

The tested compounds, **TU3**, **TU8** and **TU12** showed significant inhibition in the growth with a log reduction of 2.3, 2.0 and 2.6, respectively. These results confirm that tested compounds significantly inhibited the growth of *M. tuberculosis* in the nutrient starvation model.

2.4. *Mycobacterium tuberculosis* infected macrophage assay

When *M. tuberculosis* is ingested by macrophages, most of the bacteria are found in fused phagolysosomes, but many escapes. Thus, determining the efficiency of the molecules in this model help us to understand how the drug is inhibiting *M. tuberculosis* in the macrophages.

With this purpose, macrophages were initially infected with *M. tuberculosis*. Afterward, the cells were treated with **TU3** and **TU12**, the most active structurally different derivatives obtained from MABA and nutrient starvation model, at 10 μ M concentrations for two days. Finally, the bacterial count was performed using MPN assay. Figure 8 represents the obtained values from *M. tuberculosis* infected macrophage assay.

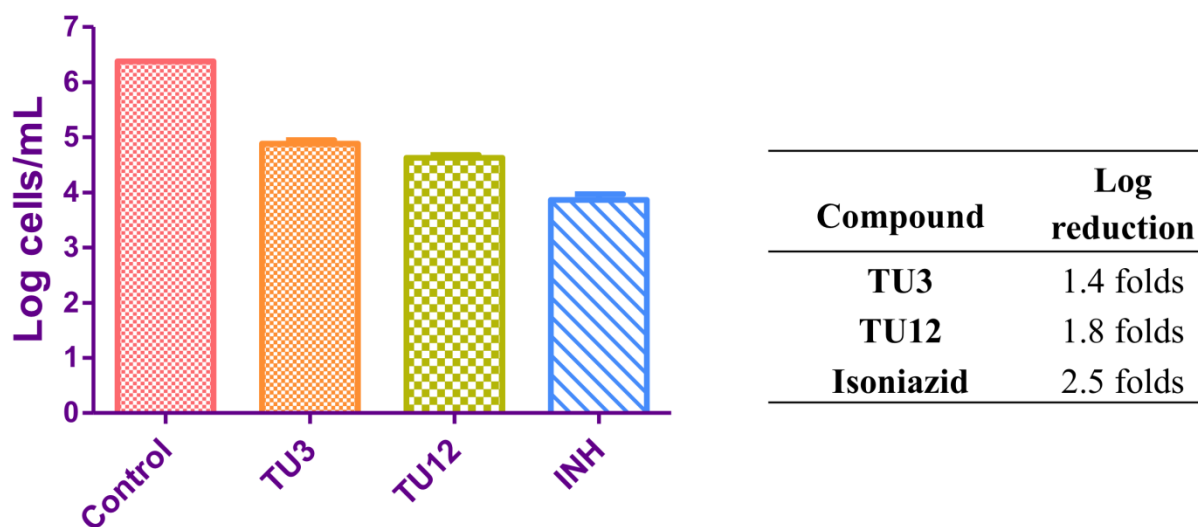


Figure 8. Comparative *M. tuberculosis* infected macrophage inhibitory activity plots. Bacterial count estimation (Mean \pm S.D., n = 4) was conducted using MPN assay.

The obtained results revealed 1.4 and 1.8 log reductions in growth, for compounds **TU3** and **TU12** respectively, compared to isoniazid (2.5 log reduction).

2.5. *InhA* inhibition assay and IC_{50} determination

The synthesized compounds carry all structural moieties required to interact with *InhA* enzyme; hydrogen bond participating atoms to form hydrogen bonds to NAD and Tyr and two hydrophobic rings. Hence, they were tested to determine their inhibition values for *InhA* from *M. tuberculosis* at 50 μ M concentration to evaluate the antimycobacterial activity mechanism.

Triclosan was used as positive control during the experiments. The compounds possessing more than 70% inhibition were also tested at 5 μ M concentration. Enzyme inhibition results are presented in Table 2.

Table 2. Enzyme inhibition values for the compounds, expressed as a percentage of InhA inhibition

Compound	% Inhibition at 50 μ M of compounds (in bracket at 5 μ M)
TU1	35
TU2	20
TU3	47
TU4	25
TU5	32
TU6	23
TU7	17
TU8	8
TU9	22
TU10	38
TU11	31
TU12	72 (25)
TU13	23
TU14	78 (29)
U1	14
U2	NI
TCL	>99 (>95)

NI: no inhibition

According to the obtained inhibition values, **TU3**, one of the compounds with the lowest MIC value in the first series, showed moderate activity with 47% inhibition. Lack of efficient InhA inhibition for the active compounds from MABA assay, **TU3**, **TU4** and **TU8**, suggests a different target for these compounds to show their antitubercular effects. Because of their strong structural similarity to thiocarlide [20], we surmise that **TU3**, **TU4** and **TU8** are likely to exhibit their antitubercular activities by targeting type II fatty acid synthase pathway via binding to HadA

through thiocarbonyl functionality in the same way as thiocarlide. Further studies must be conducted to verify this approach.

On the other side, **TU12** and **TU14** from the second subseries appeared as clearly better inhibitors of InhA with 72% and 78% inhibition values, respectively.

IC₅₀ values were also calculated for the most active InhA inhibitors, **TU12** and **TU14**, and found to be $17.7 \pm 1.3 \mu\text{M}$ and $15.6 \pm 1.6 \mu\text{M}$, respectively (Figure 9).

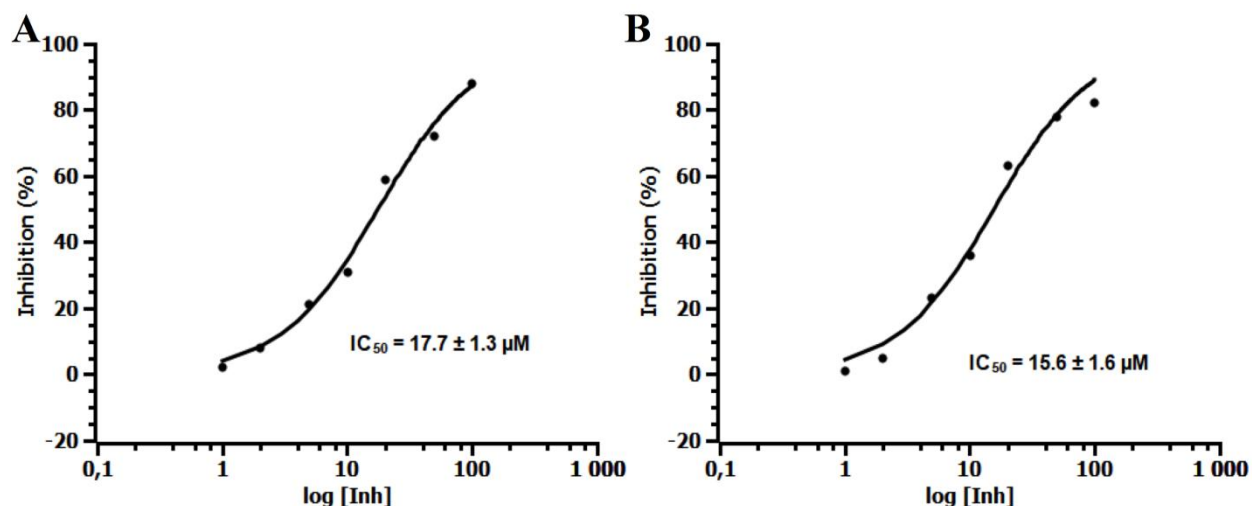


Figure 9. Determination of IC₅₀ for **TU12** (A) and **TU14** (B) against InhA enzyme

Considering the enzyme inhibition values are consistent with the results obtained from MABA assay for **TU12** and **TU14**, it can be concluded that InhA is an important target for these compounds that exhibit antimycobacterial activities.

2.6. Molecular docking

In order to support experimental InhA inhibition data with computational methods, we docked all compounds into the active pocket of InhA and illuminated their binding modes to the enzyme. The binding affinity as well as interacting amino acid residues of the enzyme with the compounds are provided as supplementary data. Here, we focus on **TU12** and **TU14**, which were found to be the most effective inhibitors of InhA. The spatial orientation and interaction patterns of **TU12** are shown in Figure 10. **TU14** has exactly the same orientation in the active pocket of InhA and 3D

interaction figure is given in supplementary material. As **TU12** and **TU14** differ from each other with only the type of the halogen they carry, molecular docking studies help us to explain their similar enzyme inhibition values. Both bromine and chlorine atoms interact with the enzyme through hydrophobic interactions.

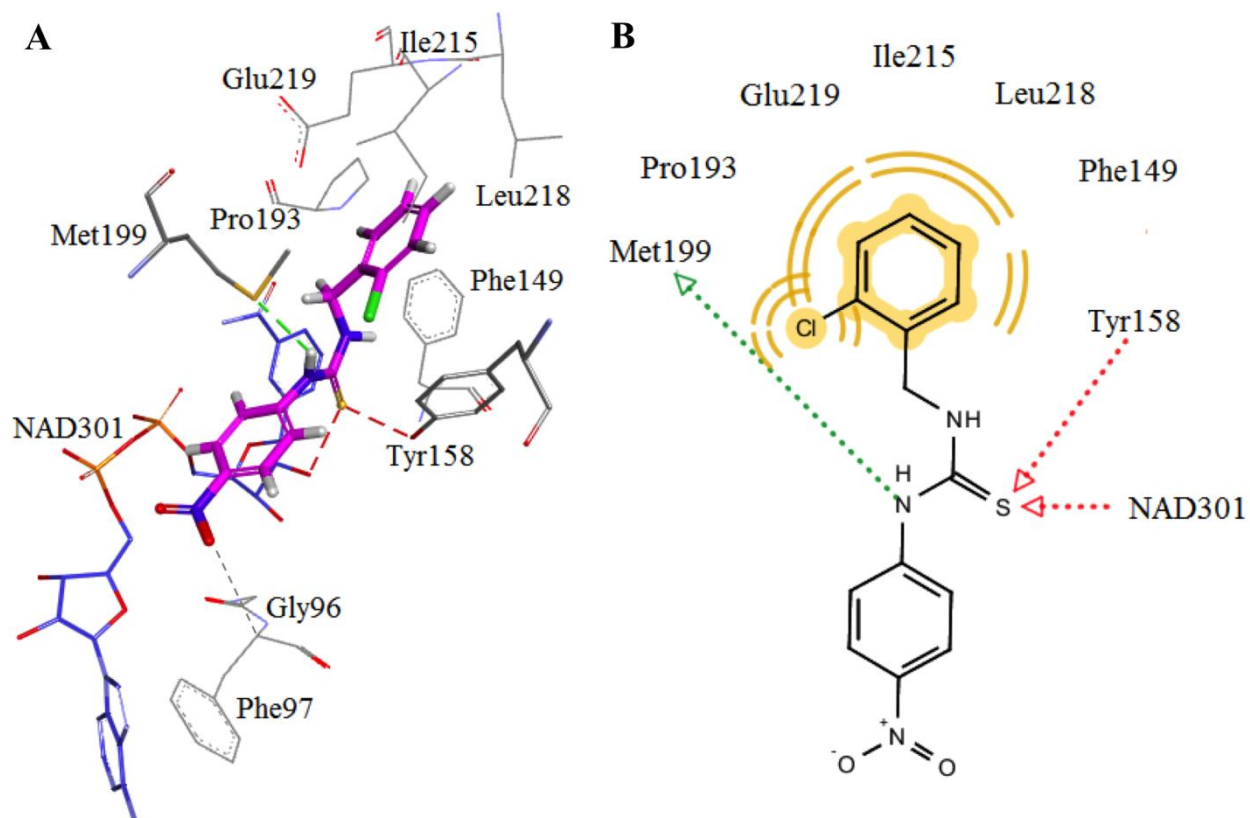


Figure 10. Proposed binding mode of **TU12** (pink stick) in the binding pocket of InhA enzyme. (A). 2D depiction of enzyme-ligand interactions: Hydrogen bond acceptor and donor interactions are represented as red and green arrows, respectively. Hydrophobic interactions are shown by yellow spheres (B).

According to the obtained interactions, **TU12** forms three key hydrogen bonds with the enzyme via the thiourea functionality. Sulfur atom of the thioketone moiety served as hydrogen bond acceptor with NAD301 and Tyr158. In thioureas, electron delocalization involving C=S and lone pairs of nitrogen atom induces an important $C^{\delta+}=S^{\delta-}$ dipole, which enables the formation resonance-induced of C=S \cdots H bonds in this functional group [21]. Additionally, **TU12** also interacted with the enzyme by forming one more hydrogen bond with the sulfur atom of Met199 through one of the nitrogen atoms of thiourea group. Benzyl moiety provided more flexibility to this compound comparing to phenyl ring and in this way, **TU12** completely occupied the

hydrophobic pocket formed by Phe149, Pro193, Ile215, Leu218, and Glu219. The chlorine atom also participated in these hydrophobic interactions. Nitrophenyl group positioned towards the phosphate groups of NAD as well as Gly96 and Phe97 at van der Waals distance. It is noteworthy that the oxygen atom of the nitro group formed non-classical hydrogen bond (C-H \cdots O) with Phe97 (represented by gray dotted lines) in this region. Although it is a weak interaction type, it can be helpful to explain why nitro derivatives are better InhA inhibitors. Consequently, **TU12** satisfies all structural requirements of well-known inhibitors of InhA enzyme. Interaction details such as bond lengths, angle and contributing amino acids for **TU12** as well as the co-crystallized ligand are summarized in Table 3.

Table 3. Interaction characteristics of **TU12** and the co-crystallized ligand of 5OIL with InhA

Compound	Interactions with amino acid residues of 5OIL		Bond Angle (°) (Tyr158, C=O, NAD301)
	Hydrogen Bonds (Bond Length-Å)	Hydrophobic Interactions	
Co-crystallized Ligand	Tyr158, (2.74), Met199 (3.66), NAD301 (2.75)	Phe149, Tyr158, Met199, Ile215, Leu218	98.06
TU12	Gly96 (3.29), Tyr158 (2.84), Met199 (2.65), NAD301 (2.81),	Phe149, Tyr158, Met199, Pro193, Ile215, Leu218, Glu219	94.79

When we analyze the interaction characteristics of original ligand of 5OIL and **TU12** with InhA, it is clear that **TU12** interacts with the enzyme through more amino acids. Compared to the co-crystallized ligand, **TU12** forms one extra hydrogen bond with InhA via Gly96. Also, the length of the hydrogen bond to Met199 of **TU12** is obviously shorter than the co-crystallized ligand's interaction. These are the determining factors that **TU12** inhibits InhA more efficiently. Additionally, the increased number of amino acids of the hydrophobic pocket interacting with **TU12** further supports the experimental enzyme inhibition data.

2.7. Structure-activity relationships

According to the data obtained from biological activity determination experiments, we summarized the structural requirements of the compounds which present antimycobacterial and InhA inhibitor activities in Figure 11.

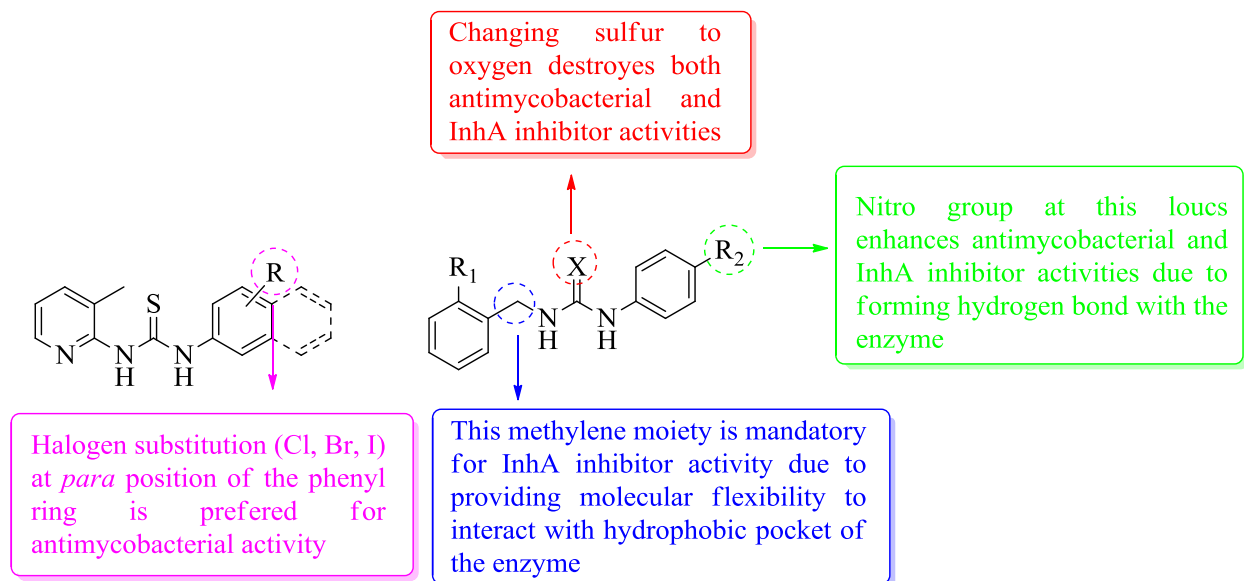


Figure 11. Structure-activity relationships of the synthesized compounds

2.8. *In silico* prediction of physicochemical properties

Some bioactive molecules may be unsuccessful to turn into good drug molecules because of low bioavailability. For this reason, molecular properties prediction can be considered as a useful tool to initially determine novel drug molecules. Herein, we applied computational methods to predict the parameters of the compounds to determine physicochemical properties. We provide the parameters of the most active compounds in Table 4. The complete table reporting about all compounds is given as supplementary data.

Table 4. Calculated physicochemical properties data of the most active compounds

Compound	LogP ^[a]	M.W. ^[b]	HBA ^[c]	HBD ^[d]	TPSA ^[e]	nROTB ^[f]	Lipinski's Violation	S ^[g] (mg/mL)
TU3	3.83	312.23	3	2	36.95	4	0	4.97
TU5	3.40	311.33	3	2	36.95	5	0	11.60
TU8	3.63	369.23	3	2	36.95	4	0	17.34
TU12	3.34	321.79	5	2	69.88	6	0	21.43
TU14	3.47	366.24	5	2	69.88	6	0	29.90

^aLogP: logarithm of *n*-octanol-water partition coefficient

^bM.W: molecular weight

^cHBA: number of hydrogen bond acceptors

^dHBD: number of hydrogen bond donors

^eTPSA: topological polar surface area

^fNROTB: number of rotatable bonds

^gS: aqueous solubility

Lipinski's rule of five is used to evaluate drug-likeness and explains the main molecular descriptors which are employed to forecast the oral bioavailability and cell permeability of novel drug candidates [22]. The newly discovered molecules must comply with at least three of these following rules: molecular weight (M.W) \leq 500 Da, *n*-octanol-water partition coefficient (log P) \leq 5, number of hydrogen bond acceptors (HBA) \leq 10, number of hydrogen bond donors (HBD) \leq 5. In addition to these descriptors, we also computed rotatable bonds (NROTB) and topological polar surface area (TPSA), which are respected to be significant parameters to determine the oral bioavailability of drug molecules [23].

According to the calculated parameters, all compounds completely adhere to Lipinski's rule of five. The active compounds are considered to be lipophilic with their calculated LogP values. Among the first-line drugs (isoniazid, ethambutol, rifampicin and pyrazinamide), only rifampicin is lipophilic. However, newly approved drugs such as bedaquiline and delamanid, additionally the molecules under clinical trials like sutezolid, clofazimine, SQ-109 and AZD-5847 are highly lipophilic [24]. This situation supports the idea that lipophilic compounds can easily penetrate through the cell wall of *M. tuberculosis*, thus lipophilic molecules have great therapeutic value as future anti-tubercular agents. TPSA values of the most active compounds were found to be 36.95 and 69.88, which are acceptable values considering that this value is below 140-150 Å² for the

most known drug molecules. Number of rotatable bonds is an important parameter which indicates molecular flexibility. In order to restrict the conformational changes while interaction with the biological target, this value should be ≤ 10 [23]. All of our compounds have less than ten rotatable bonds.

Consequently, these compounds exhibit excellent physicochemical properties to serve as antitubercular drug candidates.

3. Conclusions

Tuberculosis still causes a massive amount of deaths despite the availability of many commercial anti-TB drugs. Thus, the development of more effective and safer therapeutics is of extreme importance. With this purpose, we presented herein the rational synthesis of thiourea derivatives as antitubercular agents. We achieved effective *Mycobacterium tuberculosis* growth inhibitors, which are also capable of acting on dormant or latent forms of the bacteria. Moreover, we demonstrated that some compounds exhibit their antimycobacterial activities by inhibiting InhA enzyme, which plays a vital role in the fatty acid biosynthesis pathway in *M. tuberculosis*. Overall, thiourea can serve as an important pharmacophore in designing future therapeutics against *Mycobacterium tuberculosis* for the improvement of the treatment success rates.

4. Experimental

4.1. Chemistry

4.1.1. Materials and methods

Toluene was distilled from sodium-benzophenone just prior to use. All reagents were purchased and used as received. All volatiles were removed under the reduced pressure. Melting points were measured using open glass capillaries and are uncorrected. Infrared (IR) spectra were recorded in the range 4000–600 cm^{-1} via ATR diamond. ^1H -(400 MHz) and ^{13}C -NMR spectra (100 MHz) were obtained on a Bruker AM 400 spectrometer in (D₆) DMSO solution. Coupling constants, J , are reported in hertz. MS spectra were carried out on an LC/MS High-Resolution Time of Flight (TOF) Agilent 1200/6530 instrument at the Atatürk University-East Anatolian High Technology Research and Application Center (DAYTAM).

4.1.2. General procedure for the synthesis of the compounds

These compounds were synthesized according to the modified literature procedure [25,26]. 3-Methylpyridin-2-amine (TU1-TU10) or benzylamine derivative (TU11-TU14, U1-U2) was added to equimolar amount of corresponding phenyl/naphthyl isothiocyanate (TU1-TU14) or phenyl isocyanate (U1-U2) solutions in 10 mL dry toluene. The mixture was stirred at 80 °C and then cooled to room temperature after completion of the reaction. The precipitate was filtered off and washed with toluene. The resulting residue was purified by crystallization from ethanol to afford the target compounds.

4.1.2.1. 1-(3-Methylpyridin-2-yl)-3-phenylthiourea (TU1) [27]

Yellow solid, yield: 72%. Mp 123-124 °C; R_f (EtOAc:Hexane=4:6): 0.66. IR (ATR) 3424, 3268, 1634, 1596, 1559, 1505, 1226, 739. ^1H NMR (400 MHz, DMSO- d_6) 13.67 (s, 1H), 9.07 (s, 1H), 8.22 (d, $J = 3.9$ Hz, 1H), 7.72 (d, $J = 7.3$ Hz, 1H), 7.67 (d, $J = 7.6$ Hz, 2H), 7.39 (t, $J = 7.7$ Hz, 2H), 7.21 (t, $J = 7.2$ Hz, 1H), 7.14 – 7.07 (m, 1H), 2.35 (s, 3H). ^{13}C NMR (100 MHz, DMSO- d_6) δ 178.78 (C=S), 151.82, 143.83, 140.77, 139.26, 129.01, 126.02, 124.63, 122.35, 119.52 (aromatic carbons) and 17.01 (-CH₃). HRMS (EI): $[\text{M}+\text{H}]^+$, found 244.0887. C₁₃H₁₄N₃S requires 244.0908.

4.1.2.2. 1-(4-Methoxyphenyl)-3-(3-methylpyridin-2-yl)thiourea (TU2)

Yellow solid, yield: 32%. Mp 83-84 °C; R_f (EtOAc:Hexane=4:6): 0.45. IR (ATR) 3424, 3268, 1634, 1596, 1559, 1505, 1226, 739. ^1H NMR (400 MHz, DMSO- d_6) 13.47 (s, 1H), 8.96 (s, 1H), 8.20 (d, $J = 4.6$ Hz, 1H), 7.70 (d, $J = 7.3$ Hz, 1H), 7.52 (d, $J = 8.8$ Hz, 2H), 7.08 (dd, $J = 7.3, 5.1$ Hz, 1H), 6.94 (d, $J = 8.8$ Hz, 2H), 3.76 (s, 3H), 2.35 (s, 3H). ^{13}C NMR (100 MHz, DMSO- d_6) δ 179.01 (C=S), 157.47, 151.90, 143.80, 140.63, 132.20, 126.41, 122.10, 119.29, 114.14 (aromatic carbons) and 55.73 (-OCH₃), 17.02 (-CH₃). HRMS (EI): $[\text{M}+\text{H}]^+$, found 274.0983. C₁₄H₁₅N₃OS requires 274.1014.

4.1.2.3. 1-(2,4-Dichlorophenyl)-3-(3-methylpyridin-2-yl)thiourea (TU3)

White solid, yield: 15%. Mp 94-96 °C; R_f (EtOAc:Hexane=4:6): 0.79. IR (ATR) 3416, 2676, 1606, 1585, 1506, 1338, 1138. ^1H NMR (400 MHz, DMSO- d_6) δ 14.03 (s, 1H), 9.40 (s, 1H), 8.32 – 8.14 (m, 2H), 7.73 (d, J = 7.0 Hz, 1H), 7.69 (d, J = 2.3 Hz, 1H), 7.44 (dd, J = 8.7, 2.3 Hz, 1H), 7.24 – 7.02 (m, 1H), 2.37 (s, 3H). ^{13}C NMR (100 MHz, DMSO) δ 179.54 (C=S), 151.51, 143.60, 141.03, 135.99, 130.70, 129.23, 129.04, 128.90, 127.60, 122.48, 119.82 (aromatic carbons) and 17.03 (-CH₃). HRMS (EI): $[\text{M}+\text{H}]^+$, found 312.0095. C₁₃H₁₂Cl₂N₃S requires 312.0129.

4.1.2.4. 1-(4-Bromophenyl)-3-(3-methylpyridin-2-yl)thiourea (TU4)

White solid, yield: 59%. Mp 136-138 °C; R_f (EtOAc:Hexane=4:6): 0.28. IR (ATR) 3437, 2761, 1608, 1582, 1505, 1352, 1152. ^1H NMR (400 MHz, DMSO- d_6) δ 13.64 (s, 1H), 9.23 (s, 1H), 8.23 (d, J = 4.3 Hz, 1H), 7.73 (d, J = 7.2 Hz, 1H), 7.68 (d, J = 8.8 Hz, 2H), 7.56 (d, J = 8.7 Hz, 2H), 7.16 – 7.06 (m, 1H), 2.35 (s, 3H). ^{13}C NMR (100 MHz, DMSO) δ 178.86 (C=S), 151.72, 143.90, 140.84, 138.73, 131.78, 126.56, 122.69, 119.69, 117.98 (aromatic carbons) and 17.06 (-CH₃). HRMS (EI): $[\text{M}+\text{H}]^+$, found 321.9975. C₁₃H₁₂BrN₃S requires 322.0014.

4.1.2.5. 1-(3-Methylpyridin-2-yl)-3-(2-(trifluoromethyl)phenyl)thiourea (TU5)

White solid, yield: 81%. Mp 154-156 °C; R_f (EtOAc:Hexane=4:6): 0.10. IR (ATR) 3425, 3406, 3082, 1634, 1593, 1506, 1381, 1270, 1123. ^1H NMR (400 MHz, DMSO- d_6) δ 14.02 (s, 1H), 9.38 (s, 1H), 8.12 (d, J = 4.4 Hz, 1H), 7.90 (d, J = 8.0 Hz, 1H), 7.81 – 7.66 (m, 3H), 7.48 (t, J = 7.6 Hz, 1H), 7.11 (dd, J = 7.3, 5.1 Hz, 1H), 2.38 (s, 3H). ^{13}C NMR (100 MHz, DMSO) δ 180.76 (C=S), 151.72, 143.30, 141.00, 137.21, 132.97, 131.02, 127.24, 126.35, 124.36 (aromatic carbons), 122.74 (CF₃), 122.19, 119.63 (aromatic carbons), 16.98 (-CH₃). HRMS (EI): $[\text{M}+\text{H}]^+$, found 312.0777. C₁₃H₁₂F₃N₃S requires 312.0782.

4.1.2.6. 1-(3-Methylpyridin-2-yl)-3-(*p*-tolyl)thiourea (TU6) [28]

White solid, yield: 41%. Mp 128-129 °C; R_f (EtOAc:Hexane=4:6): 0.28. IR (ATR) 3379, 2712, 1634, 1593, 1506, 1362, 1251, 1150. ^1H NMR (400 MHz, DMSO- d_6) δ 13.58 (s, 1H), 9.02 (s, 1H), 8.22 (s, 1H), 7.72 (d, J = 7.5 Hz, 1H), 7.54 (d, J = 8.2 Hz, 2H), 7.19 (d, J = 7.9 Hz, 2H), 7.13 – 7.07 (m, 1H), 2.35 (s, 3H), 2.30 (s, 3H). ^{13}C NMR (100 MHz, DMSO) δ 178.68 (C=S), 151.87, 143.78, 140.67, 136.75, 135.19, 129.41, 124.52, 122.18, 119.34 (aromatic carbons) and 21.04, 17.02 (2x-CH₃). HRMS (EI): $[\text{M}+\text{H}]^+$, found 258.1067. C₁₄H₁₆N₃S requires 258.1065.

4.1.2.7. 1-(4-Fluorophenyl)-3-(3-methylpyridin-2-yl)thiourea (TU7)

White solid, yield: 39%. Mp 90-91 °C; R_f (EtOAc:Hexane=4:6): 0.72. IR (ATR) 3377, 2707, 1629, 1589, 1504, 1447, 1362, 1227, 1151. ^1H NMR (400 MHz, DMSO- d_6) δ 13.54 (s, 1H), 9.15 (s, 1H), 8.22 (s, 1H), 7.72 (d, $J = 7.1$ Hz, 1H), 7.69 – 7.60 (m, 2H), 7.22 (t, $J = 8.7$ Hz, 2H), 7.16 – 7.07 (m, 1H), 2.35 (s, 3H). ^{13}C NMR (100 MHz, DMSO) δ 179.30 (C=S), 160.08 (d, $^1J_{\text{F-C}} = 242.6$ Hz), 151.80, 143.88, 140.77, 135.66 (d, $^4J_{\text{F-C}} = 2.6$ Hz), 127.10 (d, $^3J_{\text{F-C}} = 8.3$ Hz), 122.47, 119.56, 115.64 (d, $^2J_{\text{F-C}} = 22.5$ Hz), 17.04 (-CH₃). HRMS (EI): $[\text{M}+\text{H}]^+$, found 262.0784. C₁₃H₁₃FN₃S requires 262.0814.

4.1.2.8. 1-(4-Iodophenyl)-3-(3-methylpyridin-2-yl)thiourea (TU8)

White solid, yield: 55%. Mp 126-128 °C; R_f (EtOAc:Hexane=4:6): 0.76. IR (ATR) 3374, 2734, 1614, 1583, 1506, 1445, 1346, 1147. ^1H NMR (400 MHz, DMSO- d_6) δ 13.63 (s, 1H), 9.21 (s, 1H), 8.22 (d, $J = 3.8$ Hz, 1H), 7.72 (d, $J = 8.2$ Hz, 3H), 7.55 (d, $J = 8.4$ Hz, 2H), 7.17 – 7.06 (m, 1H), 2.35 (s, 3H). ^{13}C NMR (100 MHz, DMSO) δ 178.75 (C=S), 151.74, 143.91, 140.86, 139.21, 137.66, 126.67, 122.70, 119.71, 90.42 (aromatic carbons) and 17.09 (-CH₃). HRMS (EI): $[\text{M}+\text{H}]^+$, found 369.9871. C₁₃H₁₃IN₃S requires 369.9875.

4.1.2.9. 1-(3,5-Bis(trifluoromethyl)phenyl)-3-(3-methylpyridin-2-yl)thiourea (TU9)

White solid, yield: 28%. Mp 139-141 °C; R_f (EtOAc:Hexane=4:6): 0.79. IR (ATR) 3445, 2249, 1622, 1052, 1024, 1005, 819. ^1H NMR (400 MHz, DMSO- d_6) δ 13.70 (s, 1H), 9.64 (s, 1H), 8.48 (s, 2H), 8.27 (s, 1H), 7.86 (s, 1H), 7.77 (s, 1H), 7.25 – 7.05 (m, 1H), 2.36 (s, 3H). ^{13}C NMR (100 MHz, DMSO) δ 179.77 (C=S), 151.36, 144.28, 141.47, 140.91, 130.78, 124.99, 123.50 (aromatic carbons), 122.28 (CF₃), 120.20, 118.58 (aromatic carbonss), 16.99 (-CH₃). HRMS (EI): $[\text{M}+\text{H}]^+$, found 380.0659. C₁₅H₁₂F₆N₃S requires 380.0656.

4.1.2.10. 1-(3-Methylpyridin-2-yl)-3-(naphthalen-2-yl)thiourea (TU10)

Pale yellow solid, yield: 75%. Mp 151-153 °C; R_f (EtOAc:Hexane=4:6): 0.69. IR (ATR) 3402, 2856, 1637, 1567, 1505, 1338, 1150. ^1H NMR (400 MHz, DMSO- d_6) δ 13.75 (s, 1H), 9.29 (s, 1H), 8.23 (d, $J = 4.9$ Hz, 1H), 8.00 (dd, $J = 6.4, 2.7$ Hz, 1H), 7.96 (d, $J = 9.1$ Hz, 1H), 7.89 (d, $J = 8.1$ Hz, 1H), 7.82 (d, $J = 7.2$ Hz, 1H), 7.77 (d, $J = 7.4$ Hz, 1H), 7.65 – 7.50 (m, 3H), 7.13 (dd, $J =$

7.4, 5.0 Hz, 1H), 2.41 (s, 3H). ^{13}C NMR (100 MHz, DMSO) δ 180.69 (C=S), 152.08, 143.88, 140.87, 135.45, 134.24, 130.19, 129.50, 128.83, 127.16, 126.70, 125.98, 124.99, 122.72, 122.45, 119.58 (aromatic carbons) and 17.16 (-CH₃). HRMS (EI): [M+H]⁺, found 294.1036. C₁₇H₁₆N₃S requires 294.1065.

4.1.2.11. 1-(2-Chlorobenzyl)-3-phenylthiourea (TU11) [29]

White solid, yield: 69%. Mp 178-180 °C; R_f (EtOAc:Hexane=4:6): 0.81. IR (ATR) 3663, 2987, 1592, 1410, 1243, 1066. ^1H NMR (400 MHz, DMSO-*d*₆) δ 9.77 (s, 1H), 8.14 (s, 1H), 7.50 – 7.41 (m, 3H), 7.40 – 7.25 (m, 5H), 7.13 (t, *J* = 7.3 Hz, 1H), 4.80 (d, *J* = 5.4 Hz, 2H). ^{13}C NMR (100 MHz, DMSO) δ 181.56 (C=S), 139.46, 136.55, 132.35, 129.56, 129.29, 129.17, 129.06, 127.55, 124.99, 123.91 (aromatic carbons) and 45.53 (-CH₂-). HRMS (EI): [M+H]⁺, found 277.0570. C₁₄H₁₄ClN₂S requires 277.0566.

4.1.2.12. 1-(2-Chlorobenzyl)-3-(4-nitrophenyl)thiourea (TU12)

Pale yellow solid, yield: 76%. Mp 148-150 °C; R_f (EtOAc:Hexane=4:6): 0.74. IR (ATR) 3674, 2987, 1594, 1529, 1508, 1407, 1302, 1240, 1066. ^1H NMR (400 MHz, DMSO-*d*₆) δ 10.38 (s, 1H), 8.65 (s, 1H), 8.19 (d, *J* = 9.2 Hz, 2H), 7.89 (d, *J* = 9.0 Hz, 2H), 7.51 – 7.44 (m, 1H), 7.44 – 7.39 (m, 1H), 7.39 – 7.26 (m, 2H), 4.82 (d, *J* = 5.1 Hz, 2H). ^{13}C NMR (100 MHz, DMSO) δ 181.13 (C=S), 146.67, 142.50, 135.80, 132.60, 129.67, 129.36, 127.63, 124.93, 121.22 (aromatic carbons, one carbon signal was overlapped) and 45.52 (-CH₂-). HRMS (EI): [M+H]⁺, found 322.0435. C₁₄H₁₃ClN₃O₂S requires 322.0417.

4.1.2.13. 1-(2-Bromobenzyl)-3-phenylthiourea (TU13)

Pale yellow solid, yield: 72%. Mp 187-189 °C; R_f (EtOAc:Hexane=4:6): 0.81. IR (ATR) 3377, 3135, 1610, 1531, 1504, 1297, 1242. ^1H NMR (400 MHz, DMSO-*d*₆) δ 9.80 (s, 1H), 8.14 (s, 1H), 7.61 (d, *J* = 7.9 Hz, 1H), 7.46 (d, *J* = 7.7 Hz, 2H), 7.43 – 7.28 (m, 4H), 7.27 – 7.19 (m, 1H), 7.20 – 7.09 (m, 1H), 4.75 (d, *J* = 4.7 Hz, 2H). ^{13}C NMR (100 MHz, DMSO) δ 181.55 (C=S), 139.45, 138.08, 132.80, 129.35, 129.29, 129.18, 128.11, 125.00, 123.90, 122.65 (aromatic carbons) and 48.01 (-CH₂-). HRMS (EI): [M+H]⁺, found 321.0045. C₁₄H₁₄BrN₂S requires 321.0061.

4.1.2.14. 1-(2-Bromobenzyl)-3-(4-nitrophenyl)thiourea (TU14)

White solid, yield: 65%. Mp 185-187 °C; R_f (EtOAc:Hexane=4:6): 0.74. IR (ATR) 3350, 3025, 1594, 1508, 1302, 1238, 1177, 1110, 1046. ^1H NMR (400 MHz, DMSO-*d*₆) δ 10.40 (s, 1H), 8.64

(s, 1H), 8.19 (d, $J = 9.2$ Hz, 2H), 7.89 (d, $J = 8.9$ Hz, 2H), 7.64 (d, $J = 8.2$ Hz, 1H), 7.48 – 7.34 (m, 2H), 7.27 – 7.20 (m, 1H), 4.78 (d, $J = 4.9$ Hz, 2H). ^{13}C NMR (100 MHz, DMSO) δ 181.14 (C=S), 146.66, 142.51, 137.35, 132.92, 129.63, 128.19, 124.94, 122.92, 121.23 (aromatic carbons one carbon signal was overlapped) and 47.98 (-CH₂-). HRMS (EI): [M+H]⁺, found 365.9937. C₁₄H₁₃BrN₃O₂S requires 365.9912.

4.1.2.15. 1-(2-Chlorobenzyl)-3-phenylurea (U1) [30]

White solid, yield: 85%. Mp 180-182 °C; R_f (EtOAc:Hexane=4:6): 0.74. IR (ATR) 3315, 2971, 1633, 1531, 1439, 1241, 1039. ^1H NMR (400 MHz, DMSO-*d*₆) δ 8.67 (s, 1H), 7.44 (dd, $J = 7.6$, 1.4 Hz, 1H), 7.42 – 7.36 (m, 3H), 7.38 – 7.25 (m, 2H), 7.22 (t, $J = 7.9$ Hz, 2H), 6.89 (t, $J = 7.3$ Hz, 1H), 6.65 (t, $J = 5.9$ Hz, 1H), 4.36 (d, $J = 6.0$ Hz, 2H). ^{13}C NMR (100 MHz, DMSO) δ 155.73 (C=O), 140.43, 137.51, 132.49, 129.59, 129.39, 129.20, 129.17, 127.68, 122.00, 118.34 (aromatic carbons) and 41.19 (-CH₂-). HRMS (EI): [M+H]⁺, found 261.0799. C₁₄H₁₄ClN₂O requires 261.0795.

4.1.2.16. 1-(2-Bromobenzyl)-3-phenylurea (U2) [31]

White solid, yield: 89%. Mp 189-191 °C; R_f (EtOAc:Hexane=4:6): 0.71. IR (ATR) 3662, 2987, 1633, 1410, 1241, 1066. ^1H NMR (400 MHz, DMSO-*d*₆) δ 8.70 (s, 1H), 7.61 (d, $J = 7.8$ Hz, 1H), 7.39 (t, $J = 6.1$ Hz, 4H), 7.28 – 7.17 (m, 3H), 6.89 (t, $J = 7.3$ Hz, 1H), 6.66 (t, $J = 5.8$ Hz, 1H), 4.32 (d, $J = 5.9$ Hz, 2H). ^{13}C NMR (100 MHz, DMSO) δ 155.59 (C=O), 140.70, 139.24, 132.81, 129.40, 129.36, 129.15, 128.23, 122.82, 121.75, 118.20 (aromatic carbons) and 43.67 (-CH₂-). HRMS (EI): [M+H]⁺, found 305.0298. C₁₄H₁₄BrN₂O requires 305.0290.

4.2. Microplate Alamar Blue Assay for *Mycobacterium tuberculosis*

In vitro antitubercular activities of the synthesized compounds were determined using Microplate Alamar Blue Assay (MABA) method. The results are stated as MIC values against *M. tuberculosis* H37Rv [32,33].

4.3. *In vitro* cytotoxicity screening

The *in vitro* cytotoxicity of the active compounds from MABA assay with MIC values $\leq 1,56$ $\mu\text{g}/\text{mL}$ were evaluated by 3-(4,5-dimethylthiazol-2-yl)-2,5-diphenyltetrazolium bromide (MTT) assay against growth inhibition of RAW 264.7 cells at 50 $\mu\text{g}/\text{mL}$ concentration [34].

4.4. Nutrient starvation model

A nutrient starvation model was applied on the bacteria by starving the culture in phosphate buffer saline (PBS) and incubating at 37 °C for six weeks. Afterward, the cultures were treated with isoniazid, rifampicin and selected compounds (10 $\mu\text{g}/\text{ml}$ concentration) for seven days. The frequency of persistors was enumerated by MPN assay [35].

4.5. Mycobacterium tuberculosis infected macrophage assay

The selected compounds were evaluated for their activities in *M. tuberculosis* infected macrophage model at 10 μM final concentration. Bacteria were suspended in 7H9 broth. Serial dilutions were performed, the plates were incubated at 37 °C and growth was observed after three weeks [33,36].

4.6. InhA inhibition and IC₅₀ determination

The InhA inhibition values of the compounds were evaluated according to the previously reported method using triclosan as a positive control. All activity assays were carried out in triplicate. IC₅₀ values were determined using the 4-parameter curve-fitting software XLFit (IDBS) with at least seven points [37,38].

Detailed experimental procedures for the biological activity evaluation studies are provided as supplementary materials.

4.7. Molecular docking

The crystal structure of Mycobacterium tuberculosis enoyl-ACP reductase (InhA) with the co-crystallized ligand 1-cyclohexyl-3-(pyridin-3-ylmethyl)urea was obtained from Protein Data Bank under the PDB code 5OIL [15]. All synthesized compounds were docked into the active pocket of the enzyme using AutoDock Vina 1.1,[39] integrated into LigandScout 4.2,[40] with default parameters. The obtained results were visually analyzed using LigandScout 4.2. The

molecular docking figures were generated by Maestro[41], DiscoveryStudio [42] and LigandScout 4.2 in this study.

4.8. In silico prediction of physicochemical properties

The chemical formulae of the compounds were drawn in ChemDraw Ultra 12.0 and saved as Simplified Molecule Input Entry System (SMILES) file. The calculation of physicochemical properties was accomplished by Molinspiration (<https://www.molinspiration.com>)[43], and Molsoft drug-likeness and molecular property prediction tool [44].

Author Statements

ŞDD and HD obtained the compounds and evaluated their structures. VSK and DS carried out MABA, nutrition starvation model, *M. tuberculosis* infected macrophage assay and cytotoxicity experiments. CL accomplished InhA inhibition assay and IC₅₀ determination. MGG was responsible for the computational studies. MGG and ŞDD wrote the manuscript.

Conflict of Interest

None of the authors declared any potential conflicts of interest.

Acknowledgements

Faculty of Pharmacy at Erciyes University is gratefully acknowledged. MGG is grateful to Prof. Dr. Gerhard Wolber, Freie Universitat Berlin, for providing the license for LigandScout 4.2.

References

- [1] S. Tiberi, M. Muñoz-Torrico, R. Duarte, M. Dalcolmo, L. D'Ambrosio, G.-B. Migliori, New drugs and perspectives for new anti-tuberculosis regimens, *Pulmonology*. 24 (2018) 86–98. doi:10.1016/J.RPPNEN.2017.10.009.
- [2] WHO | Global tuberculosis report 2019, WHO. (2019). https://www.who.int/tb/publications/global_report/en/.
- [3] D.T. Hoagland, J. Liu, R.B. Lee, R.E. Lee, New agents for the treatment of drug-resistant *Mycobacterium tuberculosis*, *Adv. Drug Deliv. Rev.* 102 (2016) 55–72. doi:10.1016/J.ADDR.2016.04.026.

- [4] K. Pyta, K. Klich, J. Domagalska, P. Przybylski, Structure and evaluation of antibacterial and antitubercular properties of new basic and heterocyclic 3-formylrifamycin SV derivatives obtained via “click chemistry” approach, *Eur. J. Med. Chem.* 84 (2014) 651–676. doi:10.1016/j.ejmech.2014.07.066.
- [5] A. Campaniço, R. Moreira, F. Lopes, Drug discovery in tuberculosis. New drug targets and antimycobacterial agents, *Eur. J. Med. Chem.* 150 (2018) 525–545. doi:10.1016/J.EJMECH.2018.03.020.
- [6] N.A. Meanwell, Synopsis of Some Recent Tactical Application of Bioisosteres in Drug Design, *J. Med. Chem.* 54 (2011) 2529–2591. doi:10.1021/jm1013693.
- [7] V. Kumar, S. Chimni, Recent Developments on Thiourea Based Anticancer Chemotherapeutics, *Anticancer. Agents Med. Chem.* 15 (2015) 163–175. doi:10.2174/1871520614666140407123526.
- [8] A. Shakeel, Thiourea Derivatives in Drug Design and Medicinal Chemistry: A Short Review, *J. Drug Des. Med. Chem.* 2 (2016) 10. doi:10.11648/j.jddmc.20160201.12.
- [9] B. Phetsuksiri, M. Jackson, H. Scherman, M. McNeil, G.S. Besra, A.R. Baulard, R.A. Slayden, A.E. DeBarber, C.E. Barry, M.S. Baird, D.C. Crick, P.J. Brennan, Unique Mechanism of Action of the Thiourea Drug Isoxyl on *Mycobacterium tuberculosis*, *J. Biol. Chem.* 278 (2003) 53123–53130. doi:10.1074/jbc.M311209200.
- [10] A.E. Grzegorzewicz, N. Eynard, A. Quémard, E.J. North, A. Margolis, J.J. Lindenberger, V. Jones, J. Korduláková, P.J. Brennan, R.E. Lee, D.R. Ronning, M.R. McNeil, M. Jackson, Covalent Modification of the *Mycobacterium tuberculosis* FAS-II Dehydratase by Isoxyl and Thiacetazone, *ACS Infect. Dis.* 1 (2016) 91–97. doi:10.1021/id500032q.
- [11] I. Pauli, R.N. dos Santos, D.C. Rostirolla, L.K. Martinelli, R.G. Ducati, L.F.S.M. Timmers, L.A. Basso, D.S. Santos, R.V.C. Guido, A.D. Andricopulo, O. Norberto de Souza, Discovery of New Inhibitors of *Mycobacterium tuberculosis* InhA Enzyme Using Virtual Screening and a 3D-Pharmacophore-Based Approach, *J. Chem. Inf. Model.* 53 (2013) 2390–2401. doi:10.1021/ci400202t.
- [12] S.D. Joshi, U.A. More, D. Koli, M.S. Kulkarni, M.N. Nadagouda, T.M. Aminabhavi, Synthesis, evaluation and in silico molecular modeling of pyrrolyl-1,3,4-thiadiazole inhibitors of InhA, *Bioorg. Chem.* 59 (2015) 151–167. doi:10.1016/j.bioorg.2015.03.001.
- [13] K. Rožman, I. Sosič, R. Fernandez, R.J. Young, A. Mendoza, S. Gobec, L. Encinas, A new ‘golden age’ for the antitubercular target InhA, *Drug Discov. Today.* 22 (2017) 492–502. doi:10.1016/J.DRUDIS.2016.09.009.
- [14] A. Chollet, L. Maveyraud, C. Lherbet, V. Bernardes-Génisson, An overview on crystal structures of InhA protein: Apo-form, in complex with its natural ligands and inhibitors, *Eur. J. Med. Chem.* 146 (2018) 318–343. doi:10.1016/J.EJMECH.2018.01.047.
- [15] F. Prati, F. Zuccotto, D. Fletcher, M.A. Convery, R. Fernandez-Menendez, R. Bates, L. Encinas, J. Zeng, C. Chung, P. De Dios Anton, A. Mendoza-Losana, C. Mackenzie, S.R. Green, M. Huggett, D. Barros, P.G. Wyatt, P.C. Ray, Screening of a Novel Fragment

Library with Functional Complexity against *Mycobacterium tuberculosis* InhA, ChemMedChem. 13 (2018) 672–677. doi:10.1002/cmdc.201700774.

- [16] G.P. Suresha, R. Suhas, W. Kapfo, D. Channe Gowda, Urea/thiourea derivatives of quinazolinone-lysine conjugates: Synthesis and structure-activity relationships of a new series of antimicrobials, Eur. J. Med. Chem. 46 (2011) 2530–2540. doi:10.1016/j.ejmech.2011.03.041.
- [17] J.M. Vega-Pérez, I. Periñán, M. Argandoña, M. Vega-Holm, C. Palo-Nieto, E. Burgos-Morón, M. López-Lázaro, C. Vargas, J.J. Nieto, F. Iglesias-Guerra, Isoprenyl-thiourea and urea derivatives as new farnesyl diphosphate analogues: Synthesis and in vitro antimicrobial and cytotoxic activities, Eur. J. Med. Chem. 58 (2012) 591–612. doi:10.1016/j.ejmech.2012.10.042.
- [18] M. Singh, P. Sasi, G. Rai, V.H. Gupta, D. Amarapurkar, P.P. Wangikar, Studies on toxicity of antitubercular drugs namely isoniazid, rifampicin, and pyrazinamide in an in vitro model of HepG2 cell line, in: Med. Chem. Res., Springer, 2011: pp. 1611–1615. doi:10.1007/s00044-010-9405-3.
- [19] A. Melamud, G.S. Kosmorsky, M.S. Lee, Ocular Ethambutol Toxicity, Mayo Clin. Proc. 78 (2003) 1409–1411. doi:10.4065/78.11.1409.
- [20] A.E. Grzegorzewicz, J. Korduláková, V. Jones, S.E.M. Born, J.M. Belardinelli, A. Vaquié, V.A.K.B. Gundi, J. Madacki, N. Slama, F. Laval, J. Vaubourgeix, R.M. Crew, B. Gicquel, M. Daffé, H.R. Morbidoni, P.J. Brennan, A. Quémar, M.R. McNeil, M. Jackson, A common mechanism of inhibition of the *Mycobacterium tuberculosis* mycolic acid biosynthetic pathway by isoxyl and thiacetazone, J. Biol. Chem. 287 (2012) 38434–38441. doi:10.1074/jbc.M112.400994.
- [21] P.A. Wood, E. Pidcock, F.H. Allen, Interaction geometries and energies of hydrogen bonds to C=O and C=S acceptors: A comparative study, Acta Crystallogr. Sect. B Struct. Sci. 64 (2008) 491–496. doi:10.1107/S0108768108015437.
- [22] C.A. Lipinski, F. Lombardo, B.W. Dominy, P.J. Feeney, Experimental and computational approaches to estimate solubility and permeability in drug discovery and development settings, Adv. Drug Deliv. Rev. 46 (2001) 3–26. doi:10.1016/S0169-409X(00)00129-0.
- [23] D.F. Veber, S.R. Johnson, H.Y. Cheng, B.R. Smith, K.W. Ward, K.D. Kopple, Molecular properties that influence the oral bioavailability of drug candidates, J. Med. Chem. 45 (2002) 2615–2623. doi:10.1021/jm020017n.
- [24] G. Piccaro, G. Poce, M. Biava, F. Giannoni, L. Fattorini, Activity of lipophilic and hydrophilic drugs against dormant and replicating *Mycobacterium tuberculosis*, J. Antibiot. (Tokyo). 68 (2015) 711–714. doi:10.1038/ja.2015.52.
- [25] Ş.D. Doğan, Copper-catalyzed NH/SH functionalization: A strategy for the synthesis of benzothiadiazine derivatives, Tetrahedron. 73 (2017) 2217–2224. doi:10.1016/J.TET.2017.02.063.
- [26] H. Doğan, Ş.D. Doğan, M.G. Gündüz, V.S. Krishna, C. Lherbet, D. Sriram, O. Şahin, E.

- Sarıpınar, Discovery of hydrazone containing thiadiazoles as *Mycobacterium tuberculosis* growth and enoyl acyl carrier protein reductase (InhA) inhibitors, *Eur. J. Med. Chem.* (2020) 112035. doi:10.1016/j.ejmech.2020.112035.
- [27] V.A. Mamedov, A.A. Kalinin, E.A. Gorbunova, W.D. Habicher, Fused polycyclic nitrogen-containing heterocycles: IX. Oxidative fusion of imidazole ring to 3-benzoylquinoxalin-2-ones, *Russ. J. Org. Chem.* 40 (2004) 1041–1046. doi:10.1023/B:RUJO.0000045201.90930.ff.
- [28] J. Valdés-Martínez, S. Hernández-Ortega, A.K. Hermetet, L.J. Ackerman, C.A. Presto, J.K. Swearingen, D.R. Kelman, K.I. Goldberg, W. Kaminsky, D.X. West, Structural studies of N-2-(3-picolyl)- and N-2-(4-picolyl)-N'-tolylthioureas, *J. Chem. Crystallogr.* 32 (2002) 431–438. doi:10.1023/A:1021136508168.
- [29] M. Mushtaque, F. Avecilla, Z. Bin Hafeez, M.M.A. Rizvi, Synthesis, Characterization, Molecular Docking, and Anticancer Evaluation of 4-Thiazolidinone Analogues, *J. Heterocycl. Chem.* 56 (2019) 1794–1805. doi:10.1002/jhet.3549.
- [30] F. Li, C. Sun, H. Shan, X. Zou, J. Xie, From Regioselective Condensation to Regioselective N-Alkylation: A Novel and Environmentally Benign Strategy for the Synthesis of N,N'-Alkyl Aryl Ureas and N,N'-Dialkyl Ureas, *ChemCatChem.* 5 (2013) 1543–1552. doi:10.1002/cctc.201200648.
- [31] X. Ran, Y. Long, S. Yang, C. Peng, Y. Zhang, S. Qian, Z. Jiang, X. Zhang, L. Yang, Z. Wang, X. Yu, A novel route to unsymmetrical disubstituted ureas and thioureas by HMPA catalyzed reductive alkylation with trichlorosilane, *Org. Chem. Front.* 7 (2020) 472–481. doi:10.1039/c9qo01321k.
- [32] L. Collins, S.G. Franzblau, Microplate alamar blue assay versus BACTEC 460 system for high-throughput screening of compounds against *Mycobacterium tuberculosis* and *Mycobacterium avium*., *Antimicrob. Agents Chemother.* 41 (1997) 1004–1009. doi:10.1128/AAC.41.5.1004.
- [33] V.S. Krishna, S. Zheng, E.M. Rekha, L.W. Guddat, D. Sriram, Discovery and evaluation of novel *Mycobacterium tuberculosis* ketol-acid reductoisomerase inhibitors as therapeutic drug leads, *J. Comput. Aided. Mol. Des.* 33 (2019) 357–366. doi:10.1007/s10822-019-00184-1.
- [34] J. van Meerloo, G.J.L. Kaspers, J. Cloos, Cell Sensitivity Assays: The MTT Assay, in: Humana Press, 2011: pp. 237–245. doi:10.1007/978-1-61779-080-5_20.
- [35] J.C. Betts, P.T. Lukey, L.C. Robb, R.A. McAdam, K. Duncan, Evaluation of a nutrient starvation model of *Mycobacterium tuberculosis* persistence by gene and protein expression profiling, *Mol. Microbiol.* 43 (2002) 717–731. doi:10.1046/j.1365-2958.2002.02779.x.
- [36] S. Biketov, G. V. Mukamolova, V. Potapov, E. Gilenkov, G. Vostroknutova, D.B. Kell, M. Young, A.S. Kaprelyants, Culturability of *Mycobacterium tuberculosis* cells isolated from murine macrophages: a bacterial growth factor promotes recovery, *FEMS Immunol. Med.*

Microbiol. 29 (2000) 233–240. doi:10.1111/j.1574-695x.2000.tb01528.x.

- [37] T. Matviiuk, J. Madacki, G. Mori, B.S. Orena, C. Menendez, A. Kysil, C. André-Barrès, F. Rodriguez, J. Korduláková, S. Mallet-Ladeira, Z. Voitenko, M.R. Pasca, C. Lherbet, M. Baltas, Pyrrolidinone and pyrrolidine derivatives: Evaluation as inhibitors of InhA and Mycobacterium tuberculosis, *Eur. J. Med. Chem.* 123 (2016) 462–475. doi:10.1016/J.EJMECH.2016.07.028.
- [38] P. Oliveira, B. Guidetti, A. Chamayou, C. André-Barrès, J. Madacki, J. Korduláková, G. Mori, B. Orena, L. Chiarelli, M. Pasca, C. Lherbet, C. Carayon, S. Massou, M. Baron, M. Baltas, Mechanochemical Synthesis and Biological Evaluation of Novel Isoniazid Derivatives with Potent Antitubercular Activity, *Molecules*. 22 (2017) 1457. doi:10.3390/molecules22091457.
- [39] O. Trott, A.J. Olson, AutoDock Vina: Improving the speed and accuracy of docking with a new scoring function, efficient optimization, and multithreading, *J. Comput. Chem.* 31 (2009) 455–461. doi:10.1002/jcc.21334.
- [40] G. Wolber, T. Langer, LigandScout: 3-D pharmacophores derived from protein-bound ligands and their use as virtual screening filters., *J. Chem. Inf. Model.* 45 (2005) 160–9. doi:10.1021/ci049885e.
- [41] Schrödinger Release 2018-3: Maestro, Schrödinger, LLC, New York, NY, 2018., (2018).
- [42] Dassault Systèmes BIOVIA, Discovery Studio Visualizer, Version 4.1.34., (2016).
- [43] Molinspiration, <https://www.molinspiration.com/cgi-bin/properties>.
- [44] Molsoft, <https://molsoft.com/mprop/>.